

Microbial Ecology and Biogeography
OF THE
Southern Ocean

David Wilkins

October 31, 2012

Contents

List of Figures	iii
List of Tables	v
List of Acronyms	vii
Acknowledgements	ix
Abstract	xi
Introduction	1
Microbial ecology of the Southern Ocean	1
Oceanography of the Southern Ocean	1
Water masses and fronts	1
Effect of climate change	1
Role of the Polar Front in biogeography	1
Project questions and hypotheses	1
The Polar Front as a major biogeographic boundary in the Southern Ocean	3
Summary	3
Introduction	3
Methods	3
Sampling and metagenomic sequencing	3
Phylogenetic analysis of metagenomic data	5
Functional analysis of metagenomic data	8
Results	9
Metagenomic sequencing	9
Phylogenetic analysis of metagenomic data	10

Functional analysis of metagenomic data	16
Discussion	17
Taxonomic groups differentiating the zones	17
Functional capacities differentiating the zones	22
Conclusions	22
Meso-scale biogeographic drivers of planktonic diversity	23
Conclusions	25

List of Figures

1	Map showing sites of seawater samples used in the Polar Front study	4
2	Rank-abundance curves for OTUs in each zone and size fraction	10
3	Contribution of Operational Taxonomic Units (OTUs) to variance between the North and South zones	13
4	Results of MINSPEC validate	15
5	Tree of GSO-EOSA-1 related 16S rRNA genes	20

List of Tables

1	Details of samples used in Polar Front study	6
2	Twenty most abundant OTUs	11
3	Highest-contributing OTUs to the difference between the North and South zones	12
4	Contributions of KEGG modules to variance between the North and South zones	18
5	Contributions of KEGG ortholog groups to variance between the North and South zones	19

Acronyms

GAAS Genome relative Abundance and Average Size.

GLPSOL GLPK LINEAR PROGRAMMING/MIP SOLVER.

ANOSIM Analysis of SIMilarities.

AOA Ammonia Oxidizing Archaea.

AZ Antarctic Zone.

CEAMARC/CASO Collaborative East Antarctic Marine Census/Climate of Southern Ocean.

CTD Conductivity, Temperature and Depth.

GLPK GNU Linear Programming Toolkit.

KEGG Kyoto Encyclopedia of Genes and Genomes.

MGI Marine Group I Crenarchaeota.

NZ North Zone.

OTU Operational Taxonomic Unit.

PF Polar Front.

PFZ Polar Frontal Zone.

SIMPERS SIMilarity PERcentages.

STF Subtropical Front.

SZ South Zone.

UFO Unidentified Flying Object.

Acknowledgements

Abstract

Introduction

This is a test of the acronyms: I saw a Unidentified Flying Object (UFO). It was not the first UFO I'd ever seen. In fact, I've seen 100 UFOs.

Here is some greek: μg .

Microbial ecology of the Southern Ocean

Oceanography of the Southern Ocean

Water masses and fronts

Effect of climate change

Role of the Polar Front in biogeography

Project questions and hypotheses

The Polar Front as a major biogeographic boundary in the Southern Ocean

Sections of this chapter have been previously published in Wilkins D., Lauro F. M., Williams T. J., DeMaere M. Z., Brown M. V., Hoffman J. M., Andrews-Pfannkoch C., McQuaid J. B., Riddle M. J., Rintoul S. R., and Cavicchioli R. (2012). Biogeographic partitioning of Southern Ocean picoplankton revealed by metagenomics. *Molecular Ecology*.

Summary

Introduction

Methods

Sampling and metagenomic sequencing

Sampling¹ was conducted on board the RSV *Aurora Australis* during cruise V3 Collaborative East Antarctic Marine Census/Climate of Southern Ocean (CEAMARC/CASO) from 13 December 2007 – 26 January 2008. This cruise occupied the SR3 latitudinal transect from Hobart, Australia (44° S) to the Mertz Glacier, Antarctica (67° S) within a longitudinal range of 140–150° E. Nineteen samples (16 surface, 3 deep) were obtained along almost the entire latitudinal range (Figure 1).

A range of data were recorded by integrated instruments on the RSV *Aurora Australis* including location, water column depth, water temperature, salinity, fluorescence and meteorological data (Table 1).

¹Sampling was performed by Jeffrey M. Hoffman and Jeffrey B. McQuaid

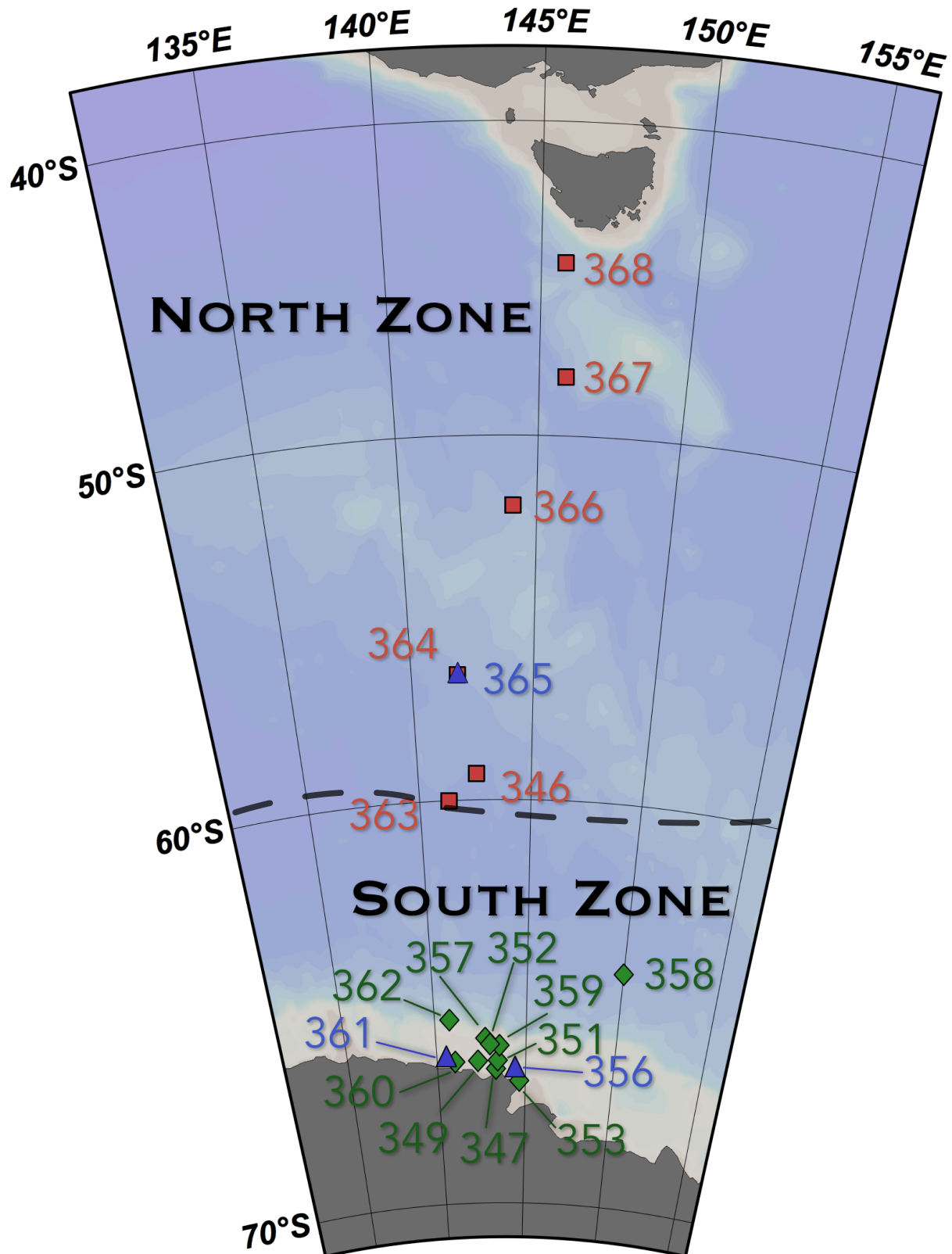


Figure 1: Sites of seawater samples used in this study. Red squares indicate surface samples from the North Zone; green diamonds samples from the South Zone; and blue triangles indicate deep samples. The dashed line gives the approximate location of the Polar Front.

These data were used to locate the Polar Frontal Zone (PFZ) based on a surface temperature gradient of ~ 1.35 °C across a distance of 45–65 km, placing the Polar Front (PF) at approximately -59.70° of latitude, consistant with previous descriptions (Moore *et al.*, 1999; Sokolov and Rintoul, 2002). Samples were accordingly grouped into “North” and “South” zones, while the three deep samples composed a “Deep” zone (Table 1). The North Zone (NZ) represents waters from the Subtropical, Subantarctic and PFZ regions, while the South Zone (SZ) represents the Antarctic Zone (AZ).

At each station, ~ 250 – 560 L of seawater was pumped from ~ 1.5 – 2.5 m below the sea surface into drums stored at ambient temperature on deck. In the case of deep samples, ~ 225 – 230 L of seawater was collected from Niskin bottles attached to a CTD (SeaBird, Bellevue, USA). Seawater samples were prefiltered through a 20 μm plankton net, then filtrate was captured on sequential 3.0 μm 0.8 μm and 0.1 μm 293 mm polyethersulfone membrane filters (Port Washington, USA), and immediately stored at -20 °C (Rusch *et al.*, 2007; Ng *et al.*, 2010).

DNA extraction² was performed at the J. Craig Venter Institute (Rockville, USA) as described in Rusch *et al.* (2007). Pyrosequencing was performed on a GS20 FLX Titanium instrument (Roche, Branford, USA) also at the J. Craig Venter Institute as described in Lauro *et al.* (2011). Duplicate reads and reads with many pyrosequencing errors were removed as described in Lauro *et al.* (2011).

Phylogenetic analysis of metagenomic data

BLAST comparison to RefSeq database

A subset of the RefSeq microbial (bacterial and archaeal) genome database (release 41, retrieved May 31 2012 from <ftp://ftp.ncbi.nih.gov/refseq/release/>) was prepared by excluding sequences with the words “shotgun”, “contig”, “partial”, “end” or “part” in their headers (Angly *et al.*, 2009). Because this database was not expected to contain representative genomes for every species present, OTUs in this study are defined by the best species match to this database, and may for example represent congeners.

The metagenomic reads from each sample were compared against this database using TBLASTX, with default parameters except for: E-value threshold 1.0×10^{-3} , cost to open gap 11, cost to extend gap 1, masking of query sequence by SEG masking with lookup table only. The outputs of all TBLASTX searches against RefSeq were processed by MINSPEC (see section following), and hits not belonging to the minimal sets were removed.

²DNA extraction was performed by Cynthia Andrews-Pfannkoch and others at the J. Craig Venter Institute

Table 1: Sampling time, location and physiochemical properties of samples used in this study. All data were retrieved from underway instruments aboard the RSV *Aurora Australis*, with the exception of temperature, salinity and fluorescence data for the three deep samples, which was obtained from the CTD (SeaBird, Bellevue, USA) instrument used to collect the samples.

Sample	Zone	Date	Latitude	Longitude	Water Column Depth (m)	Sample Depth (m)	Temperature (°C)	Salinity (PSU)	Fluorescence ($\mu\text{g L}^{-1}$)	Volume filtered (L)
346	North	20/12/07	-59.3120	142.5949	4294	2	2.9	33.75	0.3	500
347	South	23/12/07	-66.0213	142.7380	450	2	0.6	34.20	4.0	250
349	South	27/12/07	-66.5662	142.3169	370	1.5	-1.3	34.40	2.3	250
351	South	28/12/07	-66.5587	143.4303	823	1.5	-0.6	34.30	1.3	500
352	South	29/12/07	-66.7650	143.3240	164	2.5	-0.8	34.30	3.1	500
353	South	30/12/07	-67.0521	144.6786	180	2	-1.8	34.40	0.3	500
356	Deep	03/01/08	-66.7617	144.4138	920	920	-1.9	34.69	0.1	230
357	South	05/01/08	-66.1719	143.0193	580	2	-0.4	34.15	2.5	500
358	South	09/01/08	-64.3001	150.0306	3550	2	0	33.55	0.5	500
359	South	12/01/08	-66.1903	143.5292	540	2	-0.2	34.21	2.5	500
360	South	13/01/08	-66.5817	141.0211	316	2	-0.7	34.04	6.2	500
361	Deep	14/01/08	-66.4727	140.5572	1203	1170	-1.8	34.56	0.1	225
362	South	19/01/08	-65.5367	140.8287	1064	2	0.7	32.20	0.5	500
363	North	22/01/08	-60.0001	141.3094	4473	2	3.3	33.77	0.1	500
364	North	23/01/08	-56.6953	141.8780	3693	2	4	33.70	0.5	500
365	Deep	23/01/08	-56.6967	141.9125	3693	3693	0.5	34.69	0.1	230
366	North	24/01/08	-52.0233	144.1362	3180	2	7.6	33.84	0.3	500
367	North	25/01/08	-48.2487	145.9025	3490	2	11	34.43	0.2	500
368	North	26/01/08	-44.7180	145.7775	3201	2	14.8	34.96	1.3	560

Identification of minimal species sets with MINSPEC

A computational method to minimise false OTU identifications and increase the accuracy of OTU abundance estimates (MINSPEC) was developed and implemented in PERL³. Following the approach of Ye and Doak (2009) to the parsimonious reconstruction of biochemical pathways (MINPATH), MINSPEC computes the smallest set of OTUs sufficient to explain a set of observed high-quality hits against RefSeq (or any other sequence database). The minimal set computation is framed as a linear programming problem and solved with the GNU Linear Programming Toolkit (GLPK) tool GLPK LINEAR PROGRAMMING/MIP SOLVER (GLPSOL) (Free Software Foundation, Boston). This approach eliminates many of the spurious OTU identifications which result from reads with strong identity to more than one OTU. The “minimal species set” is liable to exclude some low-abundance OTUs, but gives more faithful abundance estimates and eliminates many false positives.

To validate this approach and estimate error rates, simulated microbial assemblages were generated and simulated metagenomic sampling and BLAST search was performed on each assemblage. To simulate sequence identity between taxa, each simulated taxon went through up to fifty rounds in which another taxon was selected at random and deemed to have sequence identity with the first. After each round, the this process was terminated with a 10% probability to simulate an exponential curve of interrelatedness between taxa. A random subset of the simulated taxa were then selected to form the simulated assemblage. Combined with the simulated seqence identity between taxa, this caused some taxa in the assemblage to have identity to taxa outside it. A simulated metagenomic sampling was then performed, in which a taxon was selected at random to generate a read. To simulate a natural rank-abundance curve, the randomly selected taxon would be rejected with probability $1 - \frac{1}{\ln(x)+1}$, where x is the taxon’s rank. Simulated BLAST matches to the taxon were generated for the remaining reads. Each time a taxon was selected to produce a read, other taxa with simulated sequence identity were also randomly selected to produce BLAST matches for that read, simulating the problem of a single read producing multiple matches to closely related taxa.

To fully explore the limits and reliability of MINSPEC, the simulated metagenomic experiment described above was performed with all possible permutations of the following parameters: number of simulated taxa [100; 1,000; 10,000; 50,000; 100,000]; size of simulated assemblage [1; 10; 100; 300; 500; 1,000; 10,000]; number of simulated metagenomic reads [10; 100; 1,000; 10,000; 100,000; 200,000; 500,000]. Each permutation was repeated five times, except for those where the size of the assemblage would exceed the number of taxa simulated. The resulting simulated BLAST outputs were processed with MINSPEC, and the false positive (percentage of taxa not in the assemblage which nevertheless sur-

³MINSPEC and the associated metagenomic simulation and validation scripts are open source and available at <https://github.com/wilcox/minspec>; a copy has also been provided in the supplementary information.

vived MINSPEC filtering) and false negative (percentage of taxa present in the assemblage which were not present after minspecl filtering) rates calculated. Because a high false negative rate can arise from undersampling, a problem in metagenomic studies both real and simulated, an additional “false negative (MINSPEC)” metric was calculated, which excluded taxa which were present in the assemblage but through random chance did not generate any reads, the equivalent of “unsampled rare taxa”. This rate thus represented only false negatives attributable to MINSPEC itself. Finally, as a measure of MINSPEC’s usefulness, the proportion of “false” taxa — those which generated BLAST matches but were not part of the assemblage — that were successfully removed by MINSPEC was calculated.

OTU abundances and variance between zones

The relative OTU abundances for each sample were determined using the PERL script Genome relative Abundance and Average Size (GAAS) (Angly *et al.*, 2009). Briefly, GAAS estimates the relative abundance of OTUs from the number and quality of BLAST matches to each species, taking into account differences in genome size. GAAS was run with the default settings. To normalise for reads which did not yield acceptable matches, the relative abundances for each sample were scaled by that sample’s effective BLAST hit rate. An OTU profile was generated for each sample by encoding the scaled relative abundance of each OTU from each size fraction as a separate variable.

To test the hypothesis that the oceanic zones harbour significantly different communities, Analysis of SIMilarities (ANOSIM) with 999 permutations was performed on a standardised, log-transformed Bray-Curtis resemblance matrix of OTU profiles. SIMilarity PERcentages (SIMPER) analysis was performed to identify the contribution of individual OTUs to differences between the zones. All statistical procedures were performed in PRIMER 6 as described by Clarke and Warwick (2001).

Functional analysis of metagenomic data

BLAST comparison to Kyoto Encyclopedia of Genes and Genomes (KEGG) database

In order to identify functional differences between the zones, the set of metagenomic reads from each sample was compared against the KEGG GENES database (retrieved July 2 2010 from <ftp://ftp.genome.jp/pub/kegg/genes/fasta/genes.pep>) with BLASTX, with default parameters except for: maximum number of database sequence alignments 10; E-value threshold 1.0×10^{-3} ; gap opening penalty 11; gap extension penalty 1; masking of query sequence by SEG masking for lookup table only.

Analysis of functional potential

Genes identified by BLASTX were aggregated to KEGG ortholog groups according to the KEGG Orthology schema (<ftp://ftp.genome.jp/pub/kegg/genes/ko>, retrieved Mar 29 2011), and ortholog group abundances calculated for each sample. Following Coleman and Chisholm (2010), a read was considered a hit to a given ortholog group if the top three hits for that read (or all hits if fewer than three total hits) were to genes from the same ortholog group, and had bit scores > 40. If the bit score difference between any two top hits was greater than 30, only the hits above this difference were considered.

Ortholog group counts were then used to calculate the abundance of KEGG modules. Because many ortholog groups are members of more than one module, the abundance a_m of each module m was calculated as

$$a_m = \sum_{K=1}^n \frac{C_K}{M_K}$$

where n is the number of ortholog groups K belonging to module m , C_K is the number of hits to ortholog group K , and M_K is the total number of modules to which K belongs. To account for differences in sequencing depth between samples, module abundances were scaled to 500,000 reads per sample. To test the hypothesis that the NZ and SZ harbour significantly different functional potential, one-way ANOSIM with 999 permutations was performed as above on a standardised, log-transformed Bray-Curtis distance resemblance matrix of the module and ortholog group profiles. A functional profile was generated for each sample by summing the scaled abundances of each module from all size fractions, and SIMPER performed as above to identify modules which contributed highly to the variation in functional potential between the two zones. Modules with a high contribution to variance or otherwise of interest were then linked to taxonomy (“taxonomic decomposition”) by noting the genus of the organism associated with each gene in the KEGG GENES database and thus calculating the relative contribution of each genus to each module’s abundance. This allowed functional contributions to be putatively assigned to genera which were not identified in our taxonomic analysis, as the database included gene sequences for organisms for which a full genome was not available.

Results

Metagenomic sequencing

6.6 Gbp of 454 sequence data representing picoplankton in the size range 0.1 – 3.0 µm was obtained from 16 samples. After removal of low-quality reads, 454 sequencing yielded 157,507 – 597,689 reads per sample (mean 354,399) of lengths ranging from 100 to 606 bp (mean 378).

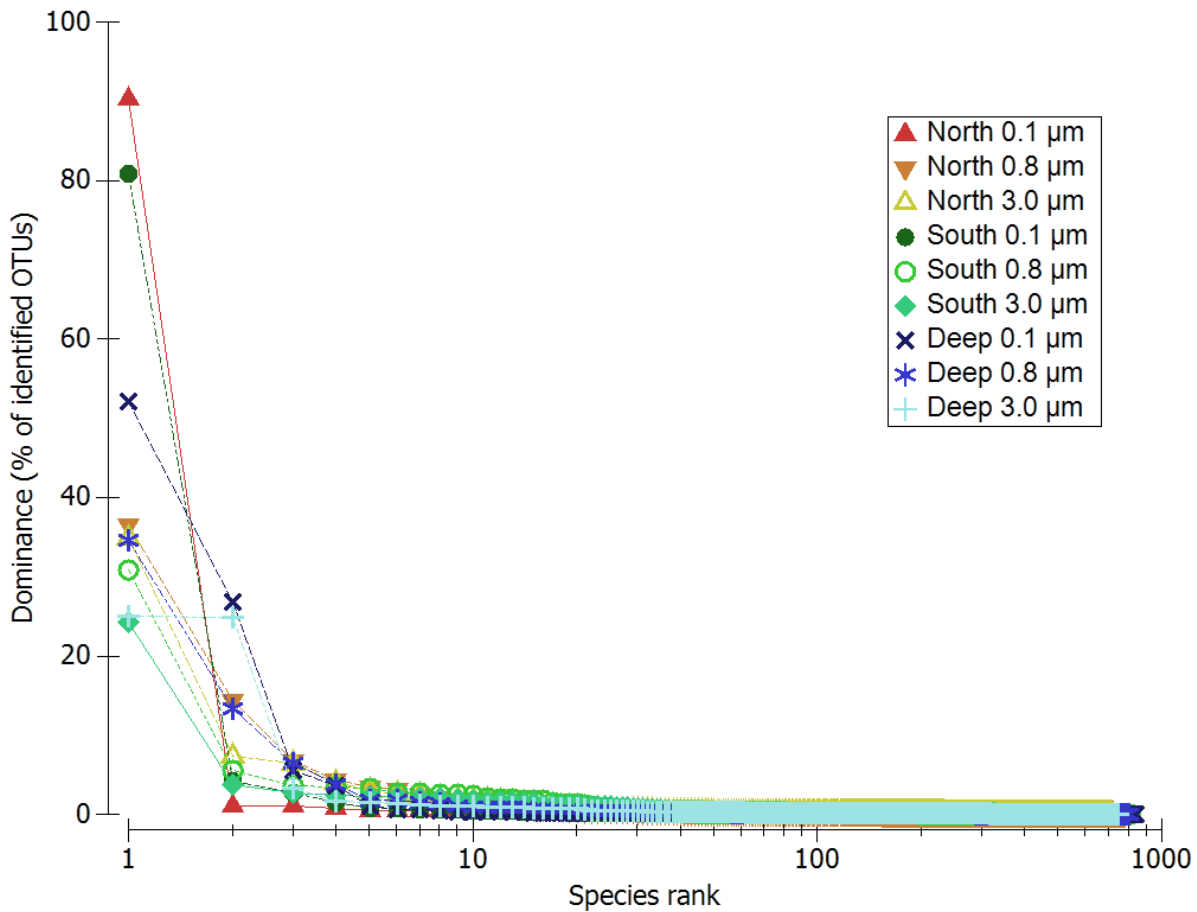


Figure 2: Rank-abundance curves for OTUs identified in each zone and size fraction. The dominance of a given OTU is its relative abundance as a percentage of all identified OTUs. The x-axis is scaled logarithmically. Generated using PRIMER 6.

Phylogenetic analysis of metagenomic data

The proportion of reads in each sample which yielded matches to RefSeq ranged from 25% to 85% (mean 62%). The most abundant OTUs in each sample are given in Table 2 and a full list of OTU abundances in the supplementary material (PF-all-OTUs.csv). All samples and size fractions exhibited very low OTU evenness (Figure 2).

ANOSIM analysis showed that the zones harbor significantly different microbial communities ($R = 0.451$, $p < 0.004$). SIMPER was performed in order to identify the contribution of individual OTUs to the difference between the NZ and SZ. The results for the highest contributors are provided in Table 3, and are graphically summarised for all OTUs in Figure 3.

The SIMPER analysis found that no single OTU contributed more than 2.9% of variance and 74% of variance was contributed by OTUs with a contribution less than 1%. There was also a large difference in the contribution to variance of the three size fractions, with approximately 52% of all variance contributed by OTUs from the 3.0 μm fraction, 37% by the 0.8 μm fraction, and 9% by the 0.1 μm

Table 2: Relative abundances (as percentages) of the twenty most abundant OTUs identified in this study, in each zone and size fraction.

OTU	North			South			Deep		
	0.1 µm	0.8 µm	3.0 µm	0.1 µm	0.8 µm	3.0 µm	0.1 µm	0.8 µm	3.0 µm
" <i>Candidatus Pelagibacter ubique</i> " HTCCC1062	61.76	25.00	23.87	58.85	22.40	17.61	37.05	24.56	17.66
<i>Nitrosopumilus maritimus</i> SCM1	0.01996	0.01438	0.009508	1.076	1.309	1.210	19.09	9.463	17.77
" <i>Candidatus Ruthia magnifica</i> " str. Cm (<i>Calyptogena magnifica</i>)	0.6699	0.6458	0.5484	2.987	2.616	1.025	3.945	4.601	2.264
<i>Roseobacter</i> sp. OCh114	0.3125	2.932	1.588	0.4477	3.994	2.657	0.1259	1.228	0.6792
<i>Synechococcus</i> sp. CC9902	0.1081	9.837	4.973	0.0007484	0.004156	0.09733	0.002846	0.01502	0.01058
<i>Silicibacter pomeroyi</i> DSS-3	0.2578	2.286	1.154	0.3070	2.505	1.576	0.1224	0.9417	0.4988
<i>Gramella forsetii</i> strain KT0803	0.2412	1.210	1.755	0.4993	2.347	1.890	0.2078	0.6179	0.5173
" <i>Candidatus Vesicomyosocius okutanii</i> " strain HA	0.4634	0.4642	0.2078	1.970	1.807	0.2174	2.480	2.662	1.167
<i>Robiginitalea biformata</i> strain HTCCC2501	0.2751	1.099	1.297	0.4722	1.878	1.405	0.2265	0.6188	0.6946
<i>Flavobacterium psychrophilum</i> strain JJP02/86	0.1718	0.8409	1.224	0.4316	1.960	1.598	0.1599	0.4744	0.6001
<i>Synechococcus</i> sp. CC9311	0.03014	4.624	4.409	0.0007221	0.02778	0.02764	0.001580	0.002863	0.009241
" <i>Candidatus Punicespirillum marinum</i> " IMCC1322	0.6444	2.077	1.267	0.3586	1.377	0.7109	0.3425	1.062	0.5345
<i>Silicibacter</i> sp. TM1040	0.2274	1.652	0.8738	0.2709	1.803	1.233	0.07665	0.5890	0.2957
<i>Jannaschia</i> sp. DFL-12	0.1776	1.378	0.7350	0.2443	1.692	0.8009	0.07338	0.6515	0.3078
<i>Zunongwangia profunda</i> strain SM-A87	0.1522	0.7487	1.059	0.2968	1.410	1.204	0.1353	0.3478	0.4971
<i>Colwellia</i> sp. 34H	0.02345	0.3636	2.736	0.05207	0.5140	1.041	0.05137	0.4687	0.8013
<i>Coralliomargarita akaiimensis</i> strain DSM 45221	0.03698	0.07573	0.1197	0.1154	1.543	1.680	0.02614	0.3040	0.2740
<i>Jannaschina</i> sp. CCS1	0.1173	0.9344	0.4784	0.1711	1.230	0.8239	0.05865	0.4462	0.2118
<i>Pseudoalteromonas atlantica</i> strain T6c	0.01251	0.4772	1.993	0.02270	0.4089	1.132	0.02634	0.2143	0.7459
<i>Saccharophagus degradans</i> strain 2-40	0.06532	0.4325	0.5429	0.1289	1.072	0.8663	0.07798	0.2844	0.3165
<i>Flavobacterium johnsoniae</i> strain UW101	0.08822	0.4220	0.6141	0.2034	0.9389	0.8578	0.07545	0.2255	0.3300
<i>Capnocytophaga ochracea</i> strain DSM 7271	0.1143	0.4830	0.5399	0.2314	0.8815	0.6814	0.08964	0.2840	0.5043
<i>Marinimonas</i> sp. MWYL1	0.03777	0.2529	0.3026	0.1514	1.300	0.7006	0.07393	0.2439	0.2155
<i>Cellvibrio japonicus</i> strain Ueda107	0.05884	0.3080	0.3231	0.1155	0.9917	0.4713	0.06774	0.2981	0.2549
<i>Marinobacter hydrocarbonoclasticus</i> VT8	0.04093	0.2889	0.3883	0.08418	0.7195	0.3848	0.1250	0.6667	1.066
<i>Pseudoalteromonas haloplanktis</i> strain TAC125	0.01389	0.2505	0.8896	0.03427	0.3561	0.6530	0.1092	1.203	0.1503
<i>Teredinibacter turnerae</i> strain T7901	0.05665	0.3051	0.3081	0.1138	0.9174	0.5127	0.06558	0.2649	0.1885
<i>Acinetobacter baumannii</i> strain SDF	0.004886	0.007187	0.4073	0.006260	0.04218	1.459	0.004285	0.01229	0.3155

Table 3: The thirty OTUs with the highest contributions to the difference between the NZ and SZ. Abundances are zonal averages and have been standardised and log-transformed. As each OTU on each size fraction was encoded as a separate variable in the SIMPER analysis, the size fraction is given after each OTU name.

OTU	Abundance South	Abundance North	Contribution to variance (%)
<i>Synechococcus</i> sp. CC9311 0.8 µm	0.00	1.08	2.88
<i>Synechococcus</i> sp. CC9902 0.8 µm	0.00	1.04	2.81
<i>Synechococcus</i> sp. CC9311 3.0 µm	0.01	0.98	2.59
<i>Synechococcus</i> sp. CC9902 3.0 µm	0.04	0.76	2.03
" <i>Candidatus Pelagibacter ubique</i> " HTCC1062 3.0 µm	1.97	2.40	1.97
" <i>Candidatus Ruthia magnifica</i> " str. Cm (<i>Calyptogena magnifica</i>) 0.1 µm	0.82	0.25	1.57
<i>Colwellia</i> sp. 34H 3.0 µm	0.34	0.66	1.32
" <i>Ca. Ruthia magnifica</i> " str. Cm (<i>Calyptogena magnifica</i>) 0.8 µm	0.74	0.25	1.32
" <i>Ca. Pelagibacter ubique</i> " HTCC1062 0.8 µm	2.32	2.48	1.32
" <i>Candidatus Vesicomyosocius okutanii</i> " strain HA 0.1 µm	0.62	0.18	1.20
<i>Coraliomargarita akajimensis</i> strain DSM 45221 0.8 µm	0.48	0.04	1.13
<i>Coraliomargarita akajimensis</i> strain DSM 45221 3.0 µm	0.49	0.06	1.10
<i>Roseobacter</i> sp. OCh114 0.8 µm	1.01	0.81	1.08
<i>Pseudoalteromonas atlantica</i> strain T6c 3.0 µm	0.38	0.54	1.08
" <i>Ca. Vesicomyosocius okutanii</i> " strain HA 0.8 µm	0.57	0.19	1.04
<i>Actinobacter baumannii</i> strain SDF 3.0 µm	0.45	0.18	0.95
<i>Gramella forsetii</i> strain KT0803 0.8 µm	0.72	0.43	0.94
<i>Martinomonas</i> sp. MWYL1 0.8 µm	0.46	0.11	0.92
<i>Roseobacter</i> sp. OCh114 3.0 µm	0.76	0.54	0.91
<i>Flavobacterium psychrophilum</i> strain JIP02/86 0.8 µm	0.63	0.32	0.89
<i>Silicibacter pomeroyi</i> DSS-3 0.8 µm	0.75	0.69	0.86
<i>Brachyspira hyodysenteriae</i> strain WA1 3.0 µm	0.47	0.19	0.84
" <i>Ca. Ruthia magnifica</i> " str. Cm (<i>Calyptogena magnifica</i>) 3.0 µm	0.34	0.21	0.82
<i>Pseudoalteromonas haloplanktis</i> strain TAC125 3.0 µm	0.22	0.33	0.77
<i>Robiginitalea biformata</i> strain HTCC2501 0.8 µm	0.61	0.40	0.74
<i>Nitrosopumilus maritimus</i> SCM1 0.1 µm	0.27	0.01	0.72
<i>Gramella forsetii</i> strain KT0803 3.0 µm	0.59	0.59	0.71
<i>Lysinibacillus sphaericus</i> strain C3-41 3.0 µm	0.29	0.02	0.71
<i>Nitrosopumilus maritimus</i> SCM1 0.8 µm	0.25	0.01	0.70
<i>Silicibacter</i> sp. TM1040 0.8 µm	0.59	0.55	0.69

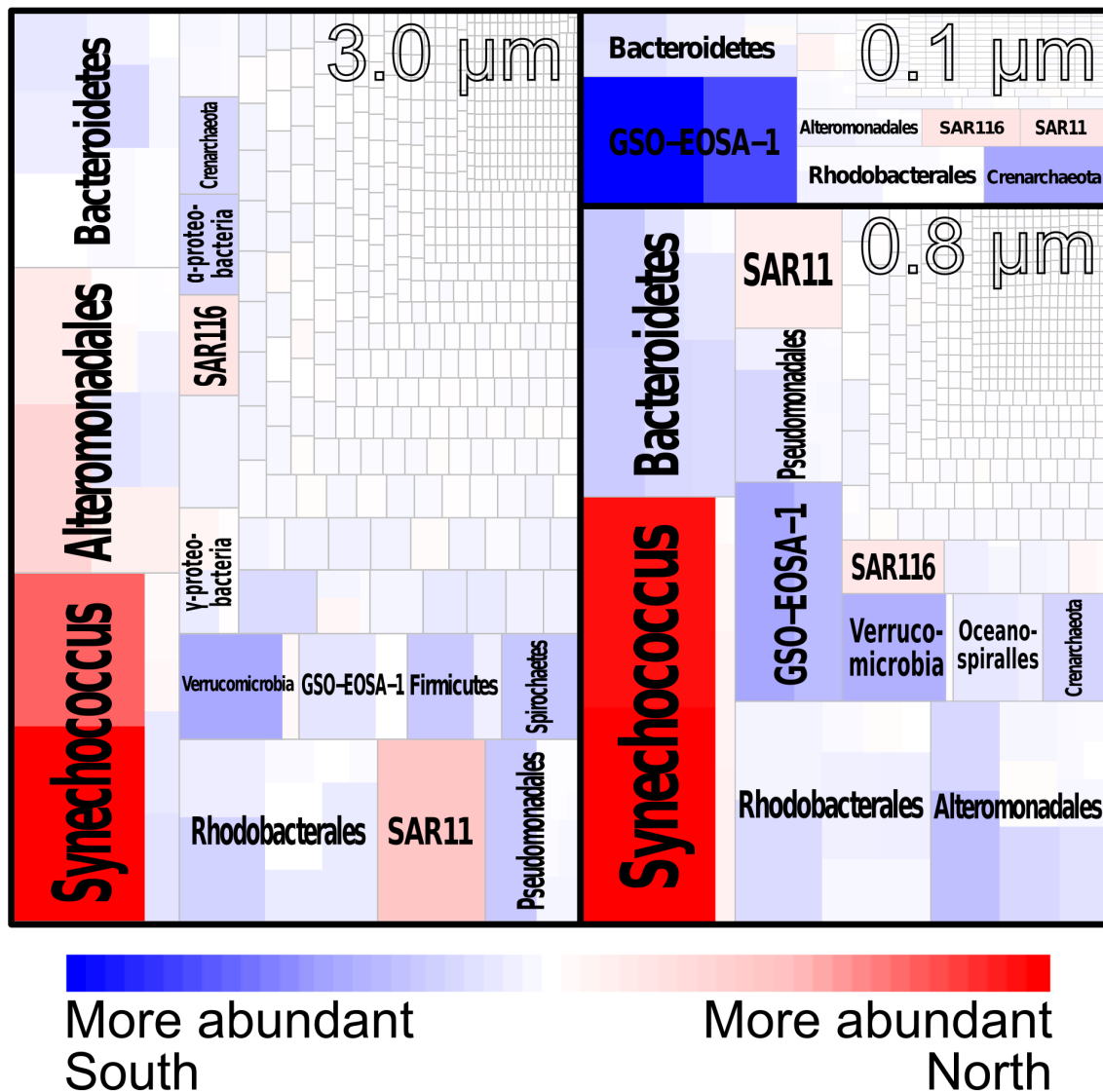


Figure 3: Contribution of OTUs to variance between the North and South zones, and differential abundance of OTUs from each size fraction between the two zones. Each coloured (red or blue) rectangle represents an OTU identified through analysis of BLAST matches between SO metagenome data and the RefSeq database. The area of each rectangle as a proportion of the total plot area corresponds to that OTU's contribution to the total variance between the two zones. The colour of each rectangle corresponds to difference in relative abundance of that OTU between the zones, with blue indicating a higher relative abundance south of the PF, and red a higher abundance north of the PF. OTUs from clades or taxonomic ranks of interest have been grouped, with labels in bold and groups separated by gray lines. Groups and OTUs with a low contribution to variance which were not grouped are unlabeled. OTUs from each size fraction have also been grouped, with labels in black outline and size fractions separated by thick black lines. The total contribution to variance of each size fraction is given as a percentage. The data used to generate this figure are given in the supplementary material (PF-OTUs-SIMPER.csv).

fraction. Notably, OTUs within several taxonomic groups that had high contribution to variance covaried in their relative representation in the NZ and SZ. For example, Bacteroidetes and GSO-EOSA-1 representatives were on average more abundant in the SZ; while *Prochlorococcus* and *Synechococcus* spp., SAR11 and SAR116 were on average more abundant in the NZ (Figure 3). Some groups, such as the Alteromonadales, had variable relative representation depending on size fraction.

Validation of MINSPEC

Repeated simulated metagenomic experiments with a wide range of permutations of parameters showed that MINSPEC was reliable and able to substantially reduce the rate of false positive OTU identifications, although its effectiveness varied with the parameters of the assemblage and metagenomic experiment.

The false negative rate, or percentage of taxa in the assemblage which were absent from the BLAST results following MINSPEC processing, was generally high, ranging from ~ 20% under ideal conditions (a low assemblage / all taxa ratio, and 500,000-read metagenomic sample) to ~ 90% in the worst case (a high assemblage / all taxa ratio and a small metagenomic sample) (Figure 4a). The assemblage / all taxa ratio (hereafter referred to as “assemblage ratio”) indicates the proportion of simulated taxa (“all taxa”) which was chosen to form the simulated assemblage. A higher ratio means it is more likely on average that any randomly selected taxon is part of the assemblage, and thus that any individual failure to detect a taxon is incorrect. This problem is mitigated with increasing the number of reads, as this makes it less likely that a given taxon would go undetected. The extreme false negative rates, in some cases 100%, represent extreme simulated scenarios (e.g. an assemblage of 1 taxon drawn from a pool of 100,000), and thus are unlikely to reflect real metagenomic studies.

Because the majority of false negatives are attributable to undersampling and failure of taxa to generate BLAST hits — properties the simulated metagenomic experiments share with real ones — a second metric, the false negative (MINSPEC) rate, was calculated (Figure 4b). This is the proportion of taxa in the assemblage which generated BLAST hits, but were incorrectly removed by MINSPEC. This rate thus represents error attributable only to MINSPEC. The false negative (MINSPEC) rate was generally low, ranging from ~ 0–1% for low assemblage ratios, to ~ 15–20% under high ratios. Surprisingly, increasing the number of reads only slightly decreased the rate, at both low and high assemblage ratios. This may be because MINSPEC requires only one read which has identity to a single taxon to ensure that taxon is not removed.

The false positive rate, or percentage of taxa not in the assemblage which nevertheless generated high-quality BLAST matches that were not removed by MINSPEC, was generally ~ 0–5% except for extremely small read sets and low assemblage ratios, where it reached as high as 60% (Figure 4c).

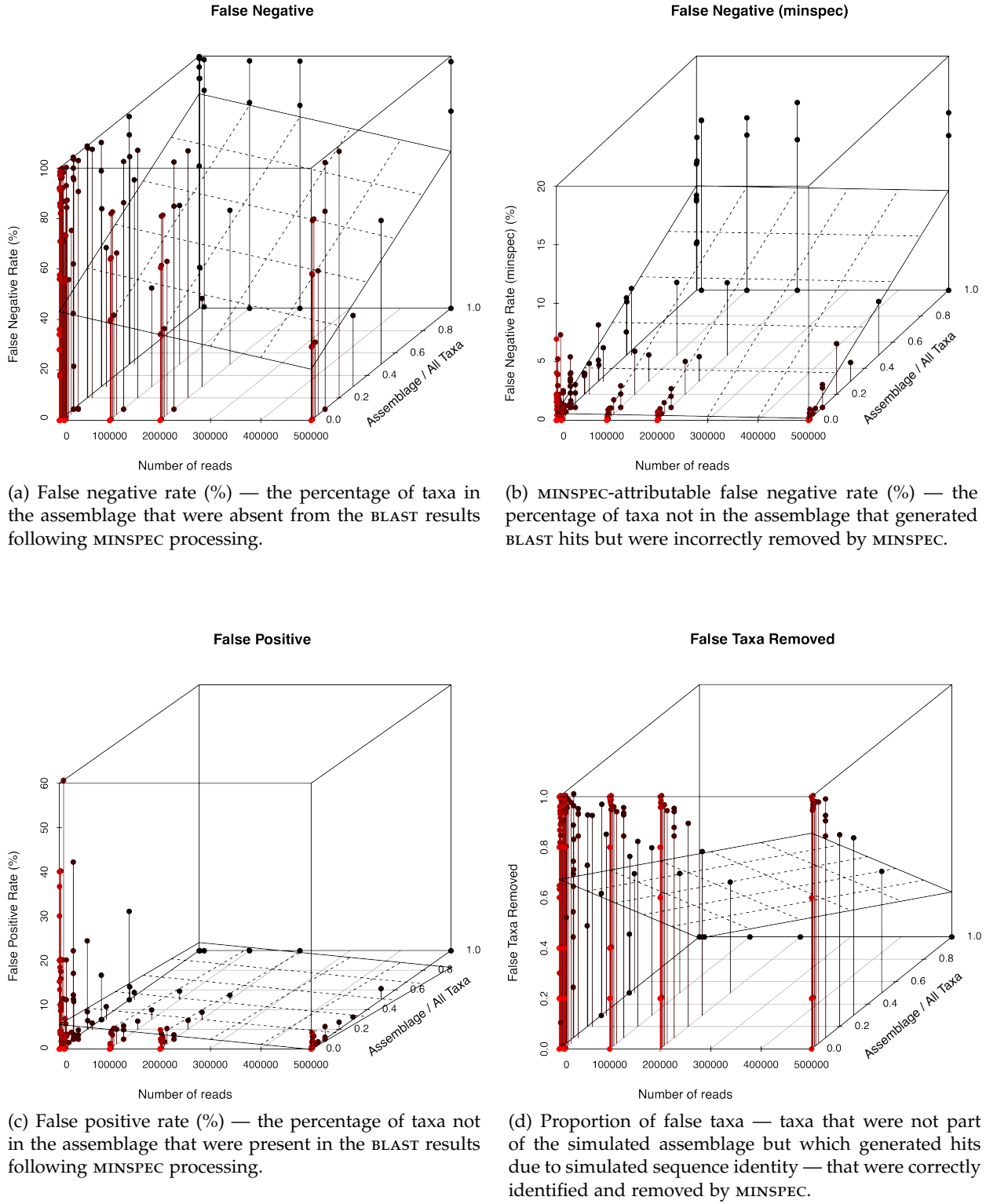


Figure 4: Results of repeated trials of MINSPEC on simulated metagenomic studies with multiple permutations of parameters (number of reads, number of simulated taxa, size of simulated assemblage). The number of simulated taxa and size of simulated assemblage are represented as a ratio on the z-axis (“assemblage / all taxa”). Each permutation was repeated five times. A plane representing a linear regression has been overlayed on each plot to indicate the trend. Points have been tinted to aid the perception of depth; colour is not otherwise meaningful.

These results reinforce the value of larger read sets, and show that once a modest metagenome size is reached ($\sim 100,000$ reads) very few false positives can be expected.

The proportion of false taxa removed was calculated to measure MINSPEC's success at identifying and eliminating taxa which are not part of the sampled assemblage yet generate high-quality BLAST matches. This rate varied from 0–1 depending on the parameters of the assemblage (Figure 4d). For simulations with a low assemblage ratio, the proportion was generally high (> 0.6), although there were simulated experiments with a low ratio where the proportion was low or zero. However, in all simulations with an assemblage ratio of 1, the proportion was 0, and the regression indicated a generally inverse relationship between the ratio and the proportion of false taxa removed. This is likely because in assemblages with a higher assemblage ratio, there are fewer false taxa to remove; in assemblages with a ratio of 1, there are none. The high proportion of false taxa correctly identified in simulations with a low assemblage ratio is thus a good indication that MINSPEC is generally successful at identifying and removing false taxa, especially as this proportion far exceeds the false positive and false negative (MINSPEC) rates for comparable experiments. As expected, increasing the number of reads improved MINSPEC's accuracy.

Overall, the simulated experiments validated both the accuracy and usefulness of MINSPEC as a tool for reducing error in metagenomic studies. It is worth noting that the assemblage ratio is not an inherent property of an assemblage, although it is limited by the assemblage's species richness. Rather, it can be decreased, and thus the accuracy of the metagenomic experiment improved, by performing BLAST searches against larger databases with finer taxonomic resolution. These results thus reinforce the value of both large read sets and comprehensive reference databases in obtaining high-quality metagenomic results.

Functional analysis of metagenomic data

ANOSIM analysis of the samples' KEGG ortholog group and module profiles revealed that the zones had significantly different functional potential (ortholog group: $R = 0.642$, $p < 0.001$; module: $R = 0.871$, $p < 0.001$). SIMPER was performed on the profiles in order to identify the specific functional differences between the zones. The highest-contributing modules are given in Table 4, and a complete list in the supplementary material (PF-modules-SIMPER.csv). The highest-contributing ortholog groups are given in Table 5, and a complete list in the supplementary material (PF-ortholog-groups-SIMPER.csv). No single ortholog group or module contributed more than 2.2% of the variance, indicating a complex and diverse pattern of functional differences. There was a strong trend for ortholog groups and modules with higher contributions to variance to be overrepresented in the NZ in the 3.0 μm fraction but the SZ in the smaller fractions, indicating that the functional diversity of each zone was strongly

segregated by size fraction.

Discussion

Taxonomic groups differentiating the zones

TODO working on this section

GSO-EOSA-1

The Gammaproteobacterial Sulfur Oxidizer-EOSA-1 (GSO-EOSA-1) cluster, represented in RefSeq by the OTUs “*Candidatus Vesicomyosocius okutanii*” strain HA and “*Candidatus Ruthia magnifica*” strain Cm. (*Calyptogena magnifica*) (Walsh *et al.*, 2009), made a large contribution to variance between the NZ and SZ, with higher abundance in the SZ: relative abundances of GSO-EOSA-1 in the SZ were 5.2%, 3.4% and 0.25% in the 0.1, 0.8 and 3.0 µm size fractions respectively, compared to 1.1%, 0.84% and 0.30% in the NZ (Table 2). The contribution to variance of this group was highest in the 0.1 µm size fraction, followed by 0.8 µm and 3.0 µm (Table 3). This pattern most likely represents a small cell size and lack of association with particulate matter.

“*Ca. R. magnifica*” and “*Ca. V. okutanii*” are chemoautotrophic endosymbionts of deep-sea bivalves (Kuwahara *et al.*, 2007; Newton *et al.*, 2007) and are thus unlikely to be present in open ocean surface waters. However, GSO-EOSA-1 representative ARCTIC96BD-19 has recently been reported at high abundance in Antarctic coastal waters (Ghilione and Murray, 2011; Grzymski *et al.*, 2012). The majority of 16S rRNA genes from this metagenome with best BLASTN matches to “*Ca. R. magnifica*” and “*Ca. V. okutanii*” clustered with ARTIC96BD-19 in a neighbour-joining phylogenetic tree (Figure 5), indicating this is the dominant GSO-EOSA-1 representative. Single-cell genomic analysis of ARCTIC96BD-19 from global mesopelagic waters indicates the lineage is probably mixotrophic, able to couple carbon fixation to oxidation of reduced sulphur compounds as well as assimilate organic carbon (Swan *et al.*, 2011). GSO-EOSA-1 cytochrome C oxidase (CoxII) has been identified in a winter metaproteome of Antarctic Peninsula coastal waters, suggesting the capacity for aerobic respiration (Williams *et al.*, 2012). Taken together, this evidence suggests the GSO-EOSA-1 representative in Antarctic coastal waters is a versatile chemolithoautotroph capable of aerobic respiration.

It has been proposed that during the winter months, chemolithoautotrophy is dominant over photoautotrophy as the major carbon fixation input in AZ waters due to the lack of available light, both from seasonal darkness and ice cover (Grzymski *et al.*, 2012). The high relative abundance of GSO-EOSA-1 we detected in SZ compared to NZ waters may therefore represent the remnants of an annual

Table 4: The thirty KEGG modules with the highest contributions to the difference between the NZ and SZ. Abundances are zonal averages and have been standardised and log-transformed.

KEGG module	Abundance South	Abundance North	Contribution to variance (%)
Photosystem II	0.42	0.57	2.21
Complex I (NADH dehydrogenase), NADH dehydrogenase I/diaphorase subunit of the bidirectional hydrogenase	0.01	0.24	1.80
Photosystem I	0.43	0.34	1.70
Pyrimidine deoxyribonucleotide biosynthesis, CDP/CTP → dCDP/dCTP,dTDP/dTTP	0.51	0.66	1.16
Histidine degradation, histidine → N-formiminoglutamate → glutamate	0.42	0.31	1.14
Methionine salvage pathway	0.29	0.43	1.14
sn-Glycerol 3-phosphate transport system	0.29	0.16	1.11
Complex I (NADH dehydrogenase), NADH dehydrogenase I	1.08	1.05	1.06
Branched-chain amino acid transport system	0.79	0.83	0.96
Dipeptide transport system	0.14	0.02	0.95
Adenine nucleotide biosynthesis, IMP → ADP/dADP,ATP/dATP	0.62	0.74	0.95
Glycine betaine/proline transport system	0.66	0.56	0.94
Sulfur reduction, sulfate → H ₂ S	0.54	0.44	0.91
Simple sugar transport system	0.46	0.39	0.90
Peptides/nickel transport system	0.99	0.98	0.89
Ribosome, eukaryotes	0.26	0.27	0.89
Multiple sugar transport system	0.55	0.55	0.86
Type II general secretion system	0.21	0.21	0.82
Sulfonate/nitrate/taurine transport system	0.45	0.37	0.82
Guanine nucleotide biosynthesis, IMP → GDP/dGDP,GTP/dGTP	0.72	0.82	0.81
RNA polymerase II, eukaryotes	0.11	0.20	0.76
Histidine biosynthesis, PRPP → histidine	0.94	0.86	0.76
Putrescine transport system	0.18	0.09	0.72
Leucine biosynthesis, pyruvate → 2-oxoisovalerate → leucine	1.29	1.37	0.71
C ₅ isoprenoid biosynthesis, non-mevalonate pathway	0.70	0.77	0.71
Leucine degradation, leucine → acetoacetate + acetyl-CoA	0.64	0.59	0.71
Thiamine transport system	0.13	0.05	0.69
Spliceosome, 35S U5-snRNP	0.18	0.20	0.68
Cytochrome b _{6f} complex	0.14	0.12	0.67
Menaquinone biosynthesis, chorismate → menaquinone	0.25	0.27	0.66

Table 5: The thirty KEGG ortholog groups with the highest contribution to the difference between the NZ and SZ. Abundances are zonal averages and have been standardised and log-transformed. As each ortholog group on each size fraction was encoded as a separate variable in the SIMPER analysis, the size fraction is given after each ortholog group name.

KEGG ortholog group	Abundance South	Abundance North	Contribution to variance (%)
Hypothetical protein 3.0 μm	0.11	0.24	0.26
Hypothetical protein 0.8 μm	0.68	0.57	0.24
Ribonucleoside-diphosphate reductase alpha chain [EC:1.17.4.1] 0.8 μm	0.17	0.24	0.15
DNA polymerase III subunit alpha [EC:2.7.7] 0.8 μm	0.25	0.19	0.14
Hypothetical protein 0.1 μm	0.26	0.24	0.12
Proline dehydrogenase / delta 1-pyrroline-5-carboxylate 0.8 μm	0.10	0.04	0.12
Aminomethyltransferase [EC:2.1.2.10] 0.8 μm	0.25	0.19	0.12
Ribonucleoside-diphosphate reductase alpha chain [EC:1.17.4.1] 3.0 μm	0.02	0.08	0.12
Sarcosine oxidase, subunit alpha [EC:1.5.3.1] 0.8 μm	0.22	0.17	0.12
Integrator complex subunit 6 3.0 μm	0.07	0.05	0.11
Multicomponent Na $^+$:H $^+$ antiporter subunit D 0.8 μm	0.11	0.05	0.11
Glutamine synthetase [EC:6.3.1.2] 0.8 μm	0.24	0.19	0.11
Pyruvate dehydrogenase E1 component [EC:1.2.4.1] 0.8 μm	0.15	0.10	0.11
Cobaltochelatase CobN [EC:6.6.1.2] 0.8 μm	0.11	0.06	0.11
Formate dehydrogenase, alpha subunit [EC:1.2.1.2] 0.8 μm	0.15	0.10	0.11
DNA-directed RNA polymerase subunit beta [EC:2.7.7.6] 3.0 μm	0.03	0.08	0.11
Glutamate synthase (NADPH/NADH) large chain [EC:1.4.1.13 1.4.1.14] 0.8 μm	0.25	0.22	0.11
Dimethylglycine dehydrogenase [EC:1.5.99.2] 0.8 μm	0.17	0.14	0.11
Flagellin 0.8 μm	0.06	0.10	0.10
DNA-directed RNA polymerase subunit beta [EC:2.7.7.6] 3.0 μm^a	0.03	0.08	0.10
Photosystem II PsbA protein 0.8 μm	0.01	0.06	0.09
Aldehyde dehydrogenase (NAD $^+$) [EC:1.2.1.3] 0.8 μm	0.17	0.13	0.09
Glutamate synthase (NADPH/NADH) large chain [EC:1.4.1.13 1.4.1.14] 3.0 μm	0.02	0.07	0.09
Thymidylylate synthase (FAD) [EC:2.1.1.148] 0.8 μm	0.02	0.06	0.09
Topoisomerase IV subunit A [EC:5.99.1.-] 0.8 μm	0.11	0.07	0.09
DNA mismatch repair protein MutS 0.8 μm	0.13	0.08	0.09
Glutamate dehydrogenase [EC:1.4.1.2] 0.8 μm	0.07	0.03	0.09
DNA polymerase I [EC:2.7.7] 0.1 μm	0.12	0.11	0.09
GTP-binding protein 0.8 μm	0.26	0.21	0.09
GTP-binding protein 3.0 μm	0.03	0.07	0.09

^aDue to an error in the KEGG database, this module is encoded twice.

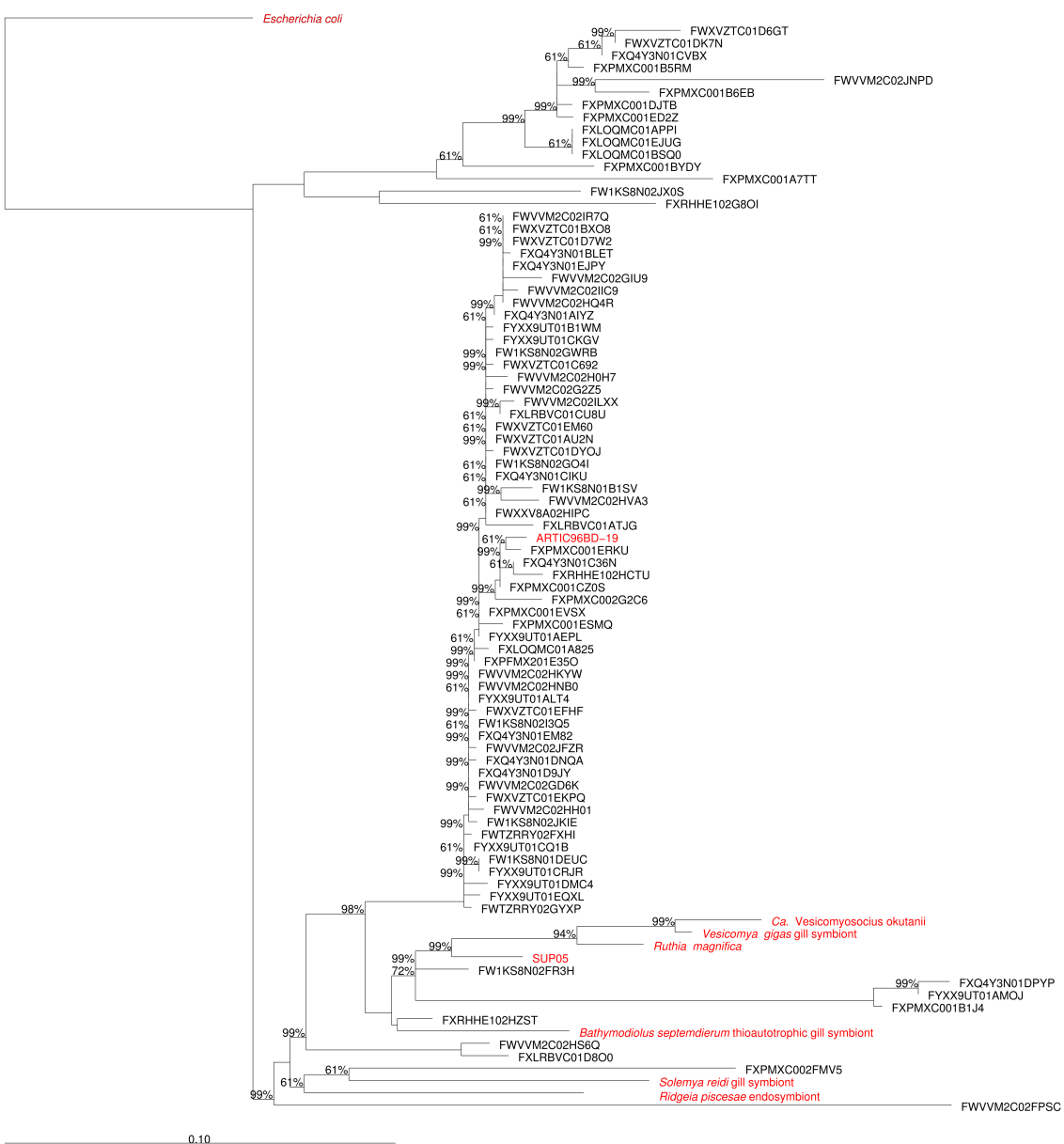


Figure 5: Neighbour-joining tree of GSO-EOSA-1-like 16S rRNA gene sequences from the metagenomes in this study. Sequences labeled in black text are reads from the metagenomes. Red labels are 16S rRNA gene sequences from Gammaproteobacterial Sulphur Oxidisers (GSO) and other gammoproteobacteria. The tree was constructed using ARB (?).

winter increase in population in the marginal ice zone which does not occur in the open ocean.

Ammonia-oxidizing Crenarchaeota

Nitrosopumilus maritimus SCM1 and *Cenarchaeum symbiosum* are chemolithoautotrophic, nitrifying members of the Marine Group I Crenarchaeota (MGI) (Preston *et al.*, 1996; Walker *et al.*, 2010) and are the only representatives in the reference database of the Ammonia Oxidizing Archaea (AOA). The contribution of OTUs of *C. symbiosum* to the AOA signature was low. As *C. symbiosum* is a sponge symbiont (Preston *et al.*, 1996) and given the poor representation of AOA in RefSeq, it is likely this OTU has attracted sequences originating from planktonic AOA and *C. symbiosum* itself is not present. AOA were moderate contributors to variance between the NZ and SZ, and were overrepresented in the SZ in all size fractions (Figure 3). As with the GSO-EOSA-1 cluster, MGI have been proposed to be abundant chemolithoautotrophs and therefore major drivers of winter carbon fixation in Antarctic coastal waters (Grzymski *et al.*, 2012; Williams *et al.*, 2012).

Sample 353 had a particularly high relative abundance of *N. maritimus* OTUs (7.5% of the 0.1 μm fraction; 0.8 μm : 11%; 3.0 μm : 12%). This sample was taken closer to the Antarctic continent (3.7 km) than any other, in relatively shallow (180 m) waters 17.6 km from the Mertz Glacier. The high abundance of ammonia oxidizers may reflect an input of ammonia from terrestrial sources (e.g. penguin guano), or resuspension of benthic sediments in which MGI are abundant (Bowman and McCuaig, 2003) by near-shore turbulence and iceberg scouring. Breakdown of water column stratification has been previously suggested as a cause of increased AOA abundance in Antarctic coastal surface waters (Kalanetra *et al.*, 2009).

Cyanobacteria

TODO begin pasted block

OTUs of the cyanobacterial genera *Prochlorococcus* and *Synechococcus* were overrepresented in the NZ in all size fractions (Figure 3). The mean relative abundance of cyanobacteria in samples 367 and 368, the two northernmost samples, was strikingly higher than the mean abundance across all other samples in the NZ. *Synechococcus* sp. CC9902 alone composed greater than 22% of the 0.8 μm fraction in these samples, consistent with *Synechococcus* species' average cell diameter of approximately 0.9 μm . The high abundance of both cyanobacterial genera on the 3.0 μm fraction has previously been reported (Lauro *et al.*, 2011) and may be attributable to aggregation (Lomas and Moran, 2011).

Samples 367 and 368 were separated from the other samples north of the PF by the Subtropical Front (STF). While the STF was not a significant boundary on the assemblage level, it may mark a significant biogeographical boundary for these cyanobacteria. *Synechococcus* and *Prochlorococcus* together

represent a large proportion of both phytoplankton abundance and carbon fixation in temperate and tropical waters, in many regions contributing more than half of total primary production (Liu *et al.*, 1997, 1998; André *et al.*, 1999). The role of the STF in determining the latitudinal range of *Synechococcus* and *Prochlorococcus* is therefore important, as it will affect models of ocean productivity under changing climactic conditions, and warrants further investigation. Despite the high abundance of cyanobacteria north of the STF, they were also a significant feature of the Subantarctic Zone (SAZ); for example, *Synechococcus* sp. CC9902 composed 3–5% of the 0.8 µm fraction in SAZ samples. Our results extend the latitudinal distribution of both *Prochlorococcus* and *Synechococcus* to include presence at very low abundance as far south as the Antarctic coast. *Prochlorococcus* have been reported to be restricted to tropical and subtropical waters within 40° of latitude (Partensky *et al.*, 1999), and to be a negligible (Ghiglione and Murray, 2011) or undetectable (Grzymski *et al.*, 2012) component of marine picoplankton in Antarctic waters. However, our findings are consistent with findings of a logarithmic relationship of cyanobacterial numbers with temperature, where cyanobacteria were found at concentrations of 10³ – 10⁴ cells per litre even in the coldest waters, approximately four orders of magnitude less than in waters around Tasmania (Marchant *et al.*, 1987). Cyanophage proteins have also been detected in a metaproteomic analysis of Antarctic Peninsula coastal surface waters (Williams *et al.*, 2012). The depth of shotgun metagenome sequence coverage of our samples is likely to have contributed to the detection of these cyanobacteria.

TODO end pasted block

TODO up to here

Functional capacities differentiating the zones

Conclusions

Meso-scale biogeographic drivers of planktonic diversity

Conclusions

References

- André J. M., Navarette C., Blanchot J., and Radenac M. H. (1999). Picophytoplankton dynamics in the equatorial Pacific: Growth and grazing rates from cytometric counts. *Journal of Geophysical Research*, 104(C2):3369–3380.
- Angly F. E., Willner D., Prieto-Davó A., Edwards R. A., Schmieder R., Vega-Thurber R., Antonopoulos D. A., Barott K., Cottrell M. T., Desnues C., Dinsdale E. A., Furlan M., Haynes M., Henn M. R., Hu Y., Kirchman D. L., McDole T., McPherson J. D., Meyer F., Miller R. M., Mundt E., Naviaux R. K., Rodriguez-Mueller B., Stevens R., Wegley L., Zhang L., Zhu B., and Rohwer F. (2009). The GAAS Metagenomic Tool and Its Estimations of Viral and Microbial Average Genome Size in Four Major Biomes. *PLoS Computational Biology*, 5(12):e1000593.
- Bowman J. P. and McCuaig R. D. (2003). Biodiversity, community structural shifts, and biogeography of prokaryotes within Antarctic continental shelf sediment. *Applied and Environmental Microbiology*, 69(5):2463–2483.
- Clarke K. R. and Warwick R. M. *Change in marine communities: an approach to statistical analysis and interpretation*. PRIMER-E, Plymouth, 2nd edition, 2001.
- Coleman M. L. M. and Chisholm S. W. S. (2010). Ecosystem-specific selection pressures revealed through comparative population genomics. *Proceedings Of The National Academy Of Sciences Of The United States Of America*, 107(43):18634–18639.
- Ghiglione J. F. and Murray A. E. (2011). Pronounced summer to winter differences and higher wintertime richness in coastal Antarctic marine bacterioplankton. *Environmental Microbiology*, 14(3): 617–629.
- Grzymski J. J., Riesenfeld C. S., Williams T. J., Dussaq A. M., Ducklow H., Erickson M., Cavicchioli R., and Murray A. E. (2012). A metagenomic assessment of winter and summer bacterioplankton from Antarctica Peninsula coastal surface waters. *The ISME Journal*, 6(10):1901–1915.
- Kalanetra K. M., Bano N., and Hollibaugh J. T. (2009). Ammonia-oxidizing Archaea in the Arctic Ocean and Antarctic coastal waters. *Environmental Microbiology*, 11(9):2434–2445.
- Kuwahara H., Yoshida T., Takaki Y., Shimamura S., Nishi S., Harada M., Matsuyama K., Takishita K., Kawato M., Uematsu K., Fujiwara Y., Sato T., Kato C., Kitagawa M., Kato I., and Maruyama T. (2007). Reduced Genome of the Thioautotrophic Intracellular Symbiont in a Deep-Sea Clam, *Calyptogena okutanii*. *Current Biology*, 17(10):881–886.
- Lauro F. M., DeMaere M. Z., Yau S., Brown M. V., Ng C., Wilkins D., Raftery M. J., Gibson J. A., Andrews-Pfannkoch C., Lewis M., Hoffman J. M., Thomas T., and Cavicchioli R. (2011). An integrative study of a meromictic lake ecosystem in Antarctica. *The ISME Journal*, 5(5):879–895.
- Liu H., Nolla H. A., and Campbell L. (1997). Prochlorococcus growth rate and contribution to primary production in the equatorial and subtropical North Pacific Ocean. *Aquatic Microbial Ecology*, 12(1): 39–47.
- Liu H., Campbell L., Landry M. R., Nolla H. A., Brown S. L., and Constantinou J. (1998). Prochlorococcus and Synechococcus growth rates and contributions to production in the Arabian Sea during the 1995 Southwest and Northeast Monsoons. *Deep Sea Research Part II: Topical Studies in Oceanography*, 45(10-11):2327–2352.

- Lomas M. W. and Moran S. B. (2011). Evidence for aggregation and export of cyanobacteria and nano-eukaryotes from the Sargasso Sea euphotic zone. *Biogeosciences*, 8(1):203–216.
- Marchant H. J., Davidson A. T., and Wright S. W. (1987). The distribution and abundance of chroococoid cyanobacteria in the Southern Ocean. *Proc. NIPR Symp. Polar Biol*, 1:1–9.
- Moore J. K., Abbott M. R., and Richman J. G. (1999). Location and dynamics of the Antarctic Polar Front from satellite sea surface temperature data. *Journal of Geophysical Research*, 104:3052–3073.
- Newton I. L. G., Woyke T., Auchtung T. A., Dilly G. F., Dutton R. J., Fisher M. C., Fontanez K. M., Lau E., Stewart F. J., Richardson P. M., Barry K. W., Saunders E., Detter J. C., Wu D., Eisen J. A., and Cavanaugh C. M. (2007). The *Calyptogena magnifica* Chemoautotrophic Symbiont Genome. *Science*, 315(5814):998–1000.
- Ng C., DeMaere M. Z., Williams T. J., Lauro F. M., Raftery M., Gibson J. A., Andrews-Pfannkoch C., Lewis M., Hoffman J. M., Thomas T., and Cavicchioli R. (2010). Metaproteogenomic analysis of a dominant green sulfur bacterium from Ace Lake, Antarctica. *The ISME Journal*, 4(8):1002–1019.
- Partensky F., Hess W. R., and Vaulot D. (1999). Prochlorococcus, a marine photosynthetic prokaryote of global significance. *Microbiology and Molecular Biology Reviews*, 63(1):106–127.
- Preston C. M., Wu K. Y., Molinski T. F., and DeLong E. F. (1996). A psychrophilic crenarchaeon inhabits a marine sponge: *Cenarchaeum symbiosum* gen. nov., sp. nov. *Proceedings Of The National Academy Of Sciences Of The United States Of America*, 93(13):6241–6246.
- Rusch D. B., Halpern A. L., Sutton G., Heidelberg K. B., Williamson S., Yooseph S., Wu D., Eisen J. A., Hoffman J. M., Remington K., Beeson K., Tran B., Smith H., Baden-Tillson H., Stewart C., Thorpe J., Freeman J., Andrews-Pfannkoch C., Venter J. E., Li K., Kravitz S., Heidelberg J. F., Utterback T., Rogers Y.-H., Falcón L. I., Souza V., Bonilla-Rosso G., Eguiarte L. E., Karl D. M., Sathyendranath S., Platt T., Bermingham E., Gallardo V., Tamayo-Castillo G., Ferrari M. R., Strausberg R. L., Nealson K., Friedman R., Frazier M., and Venter J. C. (2007). The Sorcerer II Global Ocean Sampling expedition: northwest Atlantic through eastern tropical Pacific. *PLoS Biology*, 5(3):e77–e77.
- Sokolov S. and Rintoul S. R. (2002). Structure of Southern Ocean fronts at 140°E. *Journal of Marine Systems*, 37(1):151–184.
- Swan B. K., Martinez-Garcia M., Preston C. M., Sczyrba A., Woyke T., Lamy D., Reinthaler T., Poulton N. J., Masland E. D. P., Gomez M. L., Sieracki M. E., DeLong E. F., Herndl G. J., and Stepanauskas R. (2011). Potential for Chemolithoautotrophy Among Ubiquitous Bacteria Lineages in the Dark Ocean. *Science*, 333(6047):1296–1300.
- Walker C. B., Torre J. R.de la, Klotz M. G., Urakawa H., Pinel N., Arp D. J., Brochier-Armanet C., Chain P., Chan P. P., Gollabgir A., Hemp J., Hügler M., Karr E. A., Könekke M., Shin M., Lawton T. J., Lowe T., Martens-Habbema W., Sayavedra-Soto L. A., Langf D., Sievert S. M., Rosenzweig A. C., Manning G., and Stahl D. A. (2010). Nitrosopumilus maritimus genome reveals unique mechanisms for nitrification and autotrophy in globally distributed marine crenarchaea. *Proceedings Of The National Academy Of Sciences Of The United States Of America*, 107(19):8818–8823.
- Walsh D. A., Zaikova E., Howes C. G., Song Y. C., Wright J. J., Tringe S. G., Tortell P. D., and Hallam S. J. (2009). Metagenome of a Versatile Chemolithoautotroph from Expanding Oceanic Dead Zones. *Science*, 326(5952):578–582.
- Wilkins D., Lauro F. M., Williams T. J., DeMaere M. Z., Brown M. V., Hoffman J. M., Andrews-Pfannkoch C., McQuaid J. B., Riddle M. J., Rintoul S. R., and Cavicchioli R. (2012). Biogeographic partitioning of Southern Ocean picoplankton revealed by metagenomics. *Molecular Ecology*.
- Williams T. J., Long E., Evans F., DeMaere M. Z., Lauro F. M., Raftery M. J., Ducklow H., Grzymski J. J., Murray A. E., and Cavicchioli R. (2012). A metaproteomic assessment of winter and summer bacterioplankton from Antarctic Peninsula coastal surface waters. *The ISME Journal*, 6(10):1883–1900.
- Ye Y. and Doak T. G. (2009). A parsimony approach to biological pathway reconstruction/inference for genomes and metagenomes. *PLoS Computational Biology*, 5(8):e1000465.